Interband cascade lasers grown simultaneously on GaSb, GaAs and Si substrates

Maeva Fagot, Daniel Andrés Díaz-Thomas, Audrey Gilbert, Gad Kombila, Michel Ramonda, Yves Rouillard, A. N. Baranov, Jean-Baptiste Rodriguez, Eric Tournié, Laurent Cerutti

Research Article | Vol. 32, No. 7 / 25 Mar 2024 / Optics Express 11057
Optics EXPRESS

Interband cascade lasers grown simultaneously on GaSb, GaAs and Si substrates

MAEVA FAGOT,[1] DANIEL A. DÍAZ-THOMAS,[1] AUDREY GILBERT,[1] GAD KOMBILA,[1] MICHEL RAMONDA,[2] YVES ROUILLARD,[1] ALEXEI N. BARANOV,[1] JEAN-BAPTISTE RODRIGUEZ,[1] ERIC TOURNIÉ,[1] AND LAURENT CERUTTI[1,*]

[1]*Institut d'Electronique et des Systèmes, Université de Montpellier, CNRS, F-34000 Montpellier, France*
[2]*Centrale de Technologie en Micro et nanoélectronique, Université de Montpellier, F-34000 Montpellier, France*
[*]*laurent.cerutti@umontpellier.fr*

Abstract: We report on Sb-based interband cascade lasers simultaneously grown on GaSb, GaAs and Si substrates. 8 µm x 2 mm devices exhibited similar threshold currents around 40 mA at 20°C and achieved continuous-wave (CW) operation up to 65°C on GaSb, GaAs and Si substrates despite a dislocation density of ~ 4.10^8 cm^{-2} for both mismatched substrates. In the CW regime the output power of the devices emitting at 3.3 µm exceeded 30 mW/facet at 20°C. ICLs on GaAs and Si were subsequently aged at 50°C with an injection current of 200 mA, i.e. five times the laser-threshold current. No degradation was observed after 500 h of CW operation, demonstrating the high performance of ICLs and their tolerance to dislocations.

1. Introduction

The mid-infrared (MIR) region covers wavelengths from 2 to 20 µm [1]. The 3–5 µm segment is now efficiently covered by interband cascade lasers (ICLs), which have recently been extended up to 6 µm [2,3]. Significant improvements in their design [4,5] have made ICLs the leading optoelectronic source operating in this wavelength range. They are well suited for spectroscopy applications [6,7] as this spectral region contains the absorption lines of many industrially relevant gases [4]. ICLs are also important for communications [8], medical [9,10] and defense-related applications. In addition, recent studies have demonstrated their operation beyond 14 µm [11], opening up the possibility to explore longer wavelengths.

Over the past 20 years, the integration of MIR coherent light sources on substrates such as Si and GaAs has been investigated [12]. This integration has been explored using either wafer bonding [13] or monolithic integration [14–16] and the possibility of combining the highly efficient III-V materials with the well-established silicon technology has attracted considerable interest [12,17]. By fabricating photonic integrated circuits (PICs) on such a technological platform, it becomes possible to create compact on-chip biological or chemical sensors that are relatively inexpensive, robust, and highly selective [18]. In addition, the growth of III-V lasers on Si substrates enables the low-cost mass production of devices on larger substrate sizes, providing a high scalability [12] and reducing the III-V material waste. However, several challenges must be addressed to grow high quality III-Vs films on Si substrates. The crystallographic polarity difference between the materials leads to the formation of antiphase boundaries [12], which can however be annihilated by optimizing the growth conditions [19,20]. Furthermore, the difference in lattice parameters and thermal expansion coefficients leads to the formation of a high density of dislocations [21]. They propagate through the layers forming non-radiative recombination centers hindering the performance of the devices [22,23].

#514069 https://doi.org/10.1364/OE.514069
Journal © 2024 Received 22 Nov 2023; revised 31 Jan 2024; accepted 20 Feb 2024; published 12 Mar 2024

Optics EXPRESS

Recently, however, ICLs based on type-II QWs have been shown to be tolerant to dislocations [14]. Although previous articles have reported the growth of ICLs and IC-LEDs on Si [13,14] and GaAs [16] substrates, a direct comparison between ICLs grown simultaneously on different substrates is lacking. Therefore, the purpose of this study is to present the results obtained from ICLs grown on GaSb, GaAs and Si at the same time. Several parameters have been studied in this comparative analysis, ranging from the structural properties of the grown materials to the lifetime of the lasers.

2. Growth

The ICLs structures were grown by solid-source molecular beam epitaxy (MBE) in a Riber 412 MBE system, equipped with valved As and Sb cracker cells. A 3×2 inch substrate holder was used to enable simultaneous growth on the different substrates. This approach allows direct performance comparison as all three ICLs were subjected to the same epitaxial process under identical conditions.

The first substrate employed was an n-doped ($\sim 1 \times 10^{18}\,\mathrm{cm}^{-3}$) GaSb substrate, which served as a reference. In addition, GaSb templates were grown on a GaAs substrate (Fig. 1(a)) and a Si substrate (Fig. 1(b)). The GaSb-on-GaAs was grown on an n-doped ($\sim 2 \times 10^{18}\,\mathrm{cm}^{-3}$) GaAs substrate. After deoxidation at 650°C, the temperature was lowered first to 600°C for the growth of a 200 nm thick n-GaAs buffer layer ($2 \times 10^{18}\,\mathrm{cm}^{-3}$) and then to 500°C for the growth of a 500 nm thick n-type ($1 \times 10^{18}\,\mathrm{cm}^{-3}$) GaSb layer. The APBs-free GaSb-on-Si template was grown on an n-doped ($\sim 5 \times 10^{15}\,\mathrm{cm}^{-3}$) "on-axis" Si (001) wafer with a residual offcut of 0.5° towards the (110) plane. The growth sequence that allowed us to avoid APBs in the active region of the device has been described by Rio Calvo *et al* [19]. Both templates exhibited a dislocation density in the range of $10^9\,\mathrm{cm}^{-2}$ and neither filter layers nor thermal annealing were used.

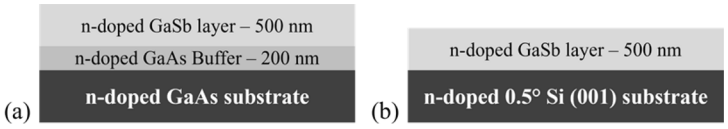

Fig. 1. Schemes of the two templates grown on (a) GaAs and (b) Si substrates.

The three different wafers were then mounted on the same substrate holder and re-introduced into the MBE system for ICL growth. After a deoxidation step at 550°C for 20 minutes, a 200 nm thick buffer layer was grown at 500°C. The growth temperature for the ICL structure was 450°C. The ICLs were designed to emit at approximately 3.3 µm, which is suitable for a variety of applications including the detection of acetone in breath analysis [24] and methane in environmental monitoring [6]. The ICL structure consists of 5 active stages sandwiched between two 400 nm Te doped ($5 \times 10^{16}\,\mathrm{cm}^{-3}$) GaSb separate confinement layers (SCLs) along with top and bottom n-doped ($6.5 \times 10^{17}\,\mathrm{cm}^{-3}$) InAs/AlSb superlattice-based claddings of 1.8 and 3 µm-thick, respectively. The ICL active zone design is described in detail by Diaz-Thomas *et al* [25].

3. Structural characterizations

After growth, the samples were characterized using high resolution X-ray diffraction (HR-XRD) to assess the crystal quality of the ICLs grown on mismatched substrates, atomic force microscopy (AFM) to evaluate the surface topology and electron channeling contrast imaging (ECCI) to estimate the threading dislocation density (TDD). The three ω-2θ diffraction patterns showed well-defined satellite peaks associated with the periodicity of the cladding superlattice and active

Optics EXPRESS

region stages. However, a broadening of the satellite peaks was observed on both GaAs and Si substrates due to the degradation of the crystal perfection induced by the dislocations (Fig. 2(a)).

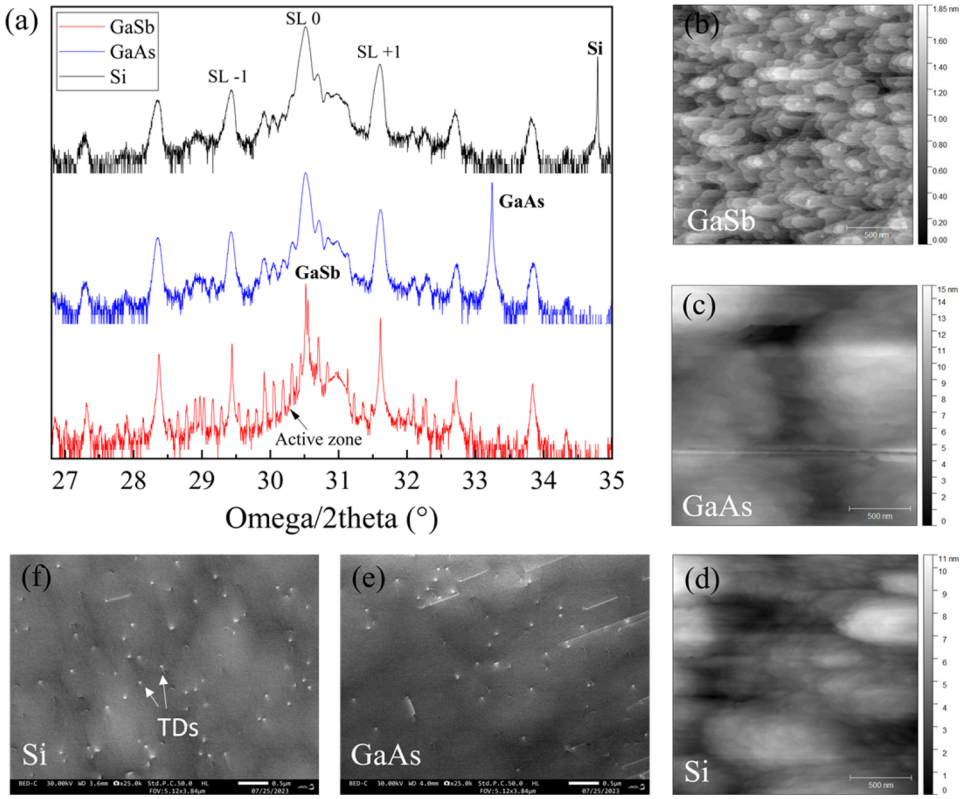

Fig. 2. (a) Comparison of the HR-XRD pattern of ICLs grown on different substrates (GaSb, GaAs and Si), 2 µm x 2 µm AFM images on (b) GaSb, (c) GaAs and (d) Si. ECCI from the surface of ICLs with a TDD higher than 10^8 cm^{-2} on (e) GaAs and (f) Si.

The ICL grown on GaSb exhibited a smooth surface with a root mean square (RMS) roughness of 0.34 nm (Fig. 2(b)), with well-defined atomic steps indicating a step-flow growth mode. Conversely, both metamorphic ICLs displayed a surface morphology revealing a spiral growth mode, attributed to the growth around the dislocation cores driven by their screw components [26]. A larger RMS roughness of 2.57 nm and 2.89 nm was measured on GaAs and Si, respectively (Fig. 2(c) and 2(d)). The ECCI images revealed a high TDD, estimated to be around 3.7×10^8 cm^{-2} and 4×10^8 cm^{-2} for the ICLs grown on GaAs and Si, respectively (Fig. 2(e) and 2(f)).

4. Wafer processing

The structures were processed into 8 µm wide ridge Fabry-Perot lasers using standard photolithography. The narrow ridges were etched down to the bottom cladding by inductively-coupled plasma reactive-ion etching (ICP-RIE) using a BCl_3-Cl_2-Ar chemistry. For all structures, including those grown on GaSb, the bottom contact was defined on top of the bottom cladding: this geometry is referred to as the top-top fabrication technique (Fig. 3(a)). Isolation and protection were then provided by hard baked AZ1518 photoresist. Contacts were made by depositing Ti/Au on top of the mesa and on the bottom cladding, as illustrated in Fig. 3(a). Finally, the lasers were cleaved to create 2 mm long cavities without facet coating, and soldered episide-up with indium onto

Optics EXPRESS

TiPtAu coated AlN submounts. The Fig. 3(b) shows scanning electron microscopy (SEM) images of an ICL on Si facet to illustrate the final device.

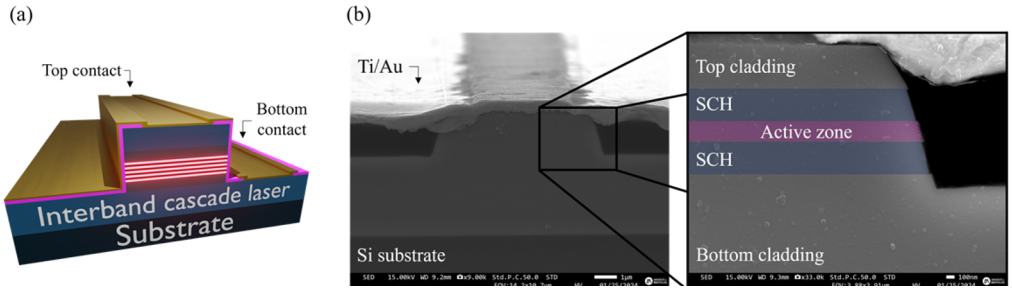

Fig. 3. (a) Ridge representation of an ICL using the top-top fabrication technique, (b) SEM images of a narrow ridge ICL on Si facet showing the device profile.

5. Electro-optical characterizations

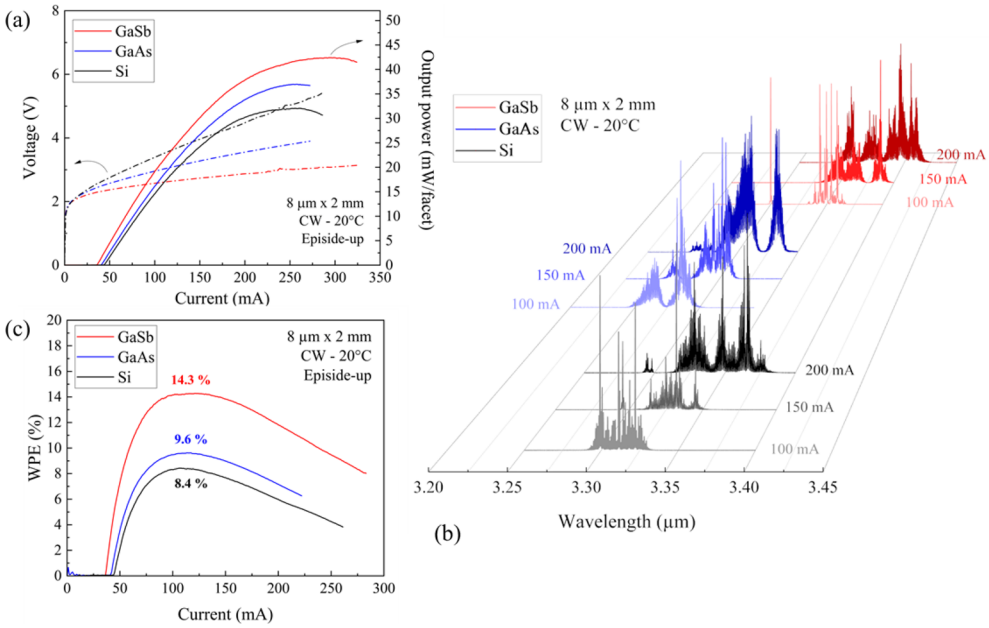

Fig. 4. (a) L-I-V curves at 20 °C in CW for 8 µm-wide ICLs on GaSb, GaAs and Si, (b) Emission spectra at 20°C for an 8 µm x 2 mm laser on various substrates at injection currents of 100, 150 and 200 mA, (c) WPE measured at 20°C in CW operation depending of the substrate type.

The performance of the ICLs in this report is representative of measurements of tens of devices measured on each substrate. The ICLs were first characterized in continuous-wave (CW) operation at 20°C. Figure 4(a) shows a comparison of the light-current-voltage (L-I-V) characteristics for the ICLs grown on the different substrates. The I-V curves exhibit a consistent turn-on voltage of 2.3 V, and similar threshold currents were observed for all lasers, ranging from 36 mA on GaSb to 45 mA on Si. However, as the lattice mismatch increases, the series resistance (R_s) increases significantly: approximately 3 Ω for GaSb, 6 Ω for GaAs and 11 Ω

Optics EXPRESS

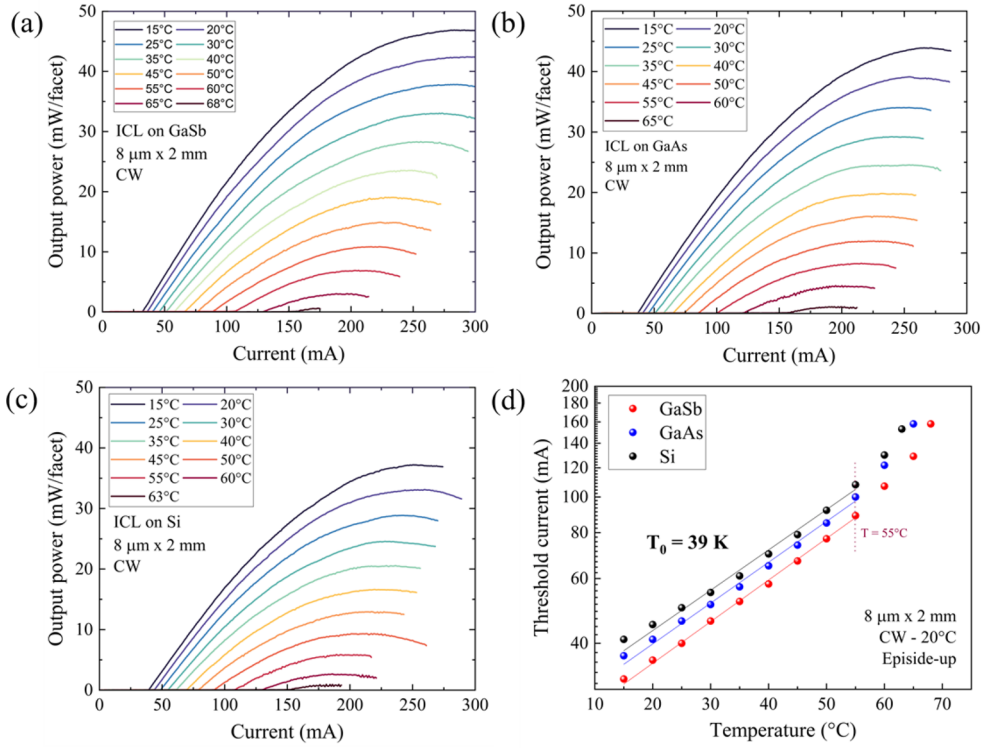

Fig. 5. Temperature dependent L-I curves measured in CW of 8 µm x 2 mm ICLs on (a) GaSb, (b) GaAs and (c) Si, (d) Evolution of the threshold current as a function of the operating temperature on the three substrates.

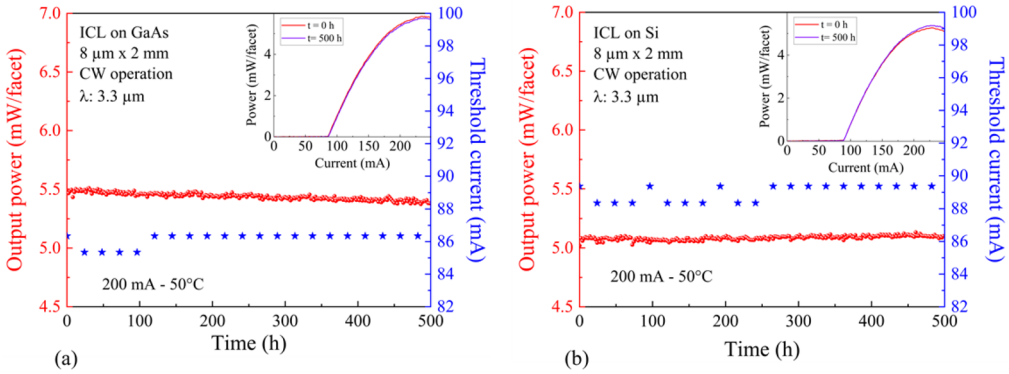

Fig. 6. Ageing data measured at 50°C under a current injection of 200 mA for ICLs (a) on GaAs (b) on Si. Inset: L-I curves of the ICL at the beginning and end of the ageing.

Optics EXPRESS

for Si. This increase in R_s affects the temperature inside the device and therefore the maximum optical power. On GaSb, the maximum output power value is 42 mW/facet, on GaAs it is reduced to 37 mW/facet, and on Si it drops down to 32 mW/facet. The CW emission spectra measured at 20°C for three injection currents (100, 150 and 200 mA) are plotted in Fig. 4(b). The central emission is between 3.25 and 3.42 µm, close to the target wavelength expected from the design.

The wall-plug efficiency (WPE) was calculated from the L-I-V characteristics of the devices and Fig. 4(c) depicts the evolution of the WPE with the current. The maximum value decreases from 14.3% for GaSb to 9.6% and 8.4% for GaAs and Si, respectively.

The temperature dependent L-I curves of the ICLs on GaSb, GaAs and Si are shown in Fig. 5(a), (b) and (c) respectively. The maximum operating temperatures were 65 and 63°C on GaAs and Si respectively, whereas it reached 68°C for the ICLs grown on GaSb. Figure 5(d) shows the temperature dependence of the threshold. Up to 55°C, the same characteristic temperature T_0 of 39 K was extracted, independently of the substrate. The evaluation of the threshold voltage as a function of temperature shows that at room temperature, the voltage efficiency on GaSb is at the state-of-the-art (80.4%), while on GaAs and Si it is of 74% and 68.5% respectively. There is a 12% difference between the voltage efficiencies of ICLs on GaSb and Si, which is related to the high series resistance. At a higher temperature (60°C) the value drops to 74.3% on GaSb, 61.5% on GaAs and 50.4% on Si, with a maximum difference of 24%.

Finally, ICLs on GaAs and Si were aged at 50°C under CW operation with an injection current as high as 200 mA. The results are plotted in Fig. 6. No degradation was observed after 500 h on either substrate, meaning that longer ageing times are required to extrapolate the mean time to failure (MTTF) [22,27].

6. Discussion

In the previous section, the electro-optical characteristics of ICLs grown on both native and non-native substrates were investigated. It was observed that the threshold current is similar for all lasers, around 40 mA. However, there is a notable difference in the series resistance between GaSb and mismatched substrates. This discrepancy could be attributed to the lower lateral electrical conductivity caused by the presence of threading dislocations in the bottom cladding. Interestingly, the TDD on both GaAs and Si is comparable at around 4×10^8 cm^{-2}. The high series resistance introduces additional Joule heating, which increases the temperature in the active zone. This effect has a direct impact on the threshold voltage and optical output power by reducing its maximum value, as seen in the previous section. The difference in R_s prompts further investigation to gain a deeper insight into this aspect. Assuming that this electrical problem can be solved, ICLs on mismatched substrates will outperform those on GaSb due to their higher thermal conductivity (0.33, 0.55, and 1.3 W/cm°C on GaSb, GaAs and Si, respectively). We also observed a blue shift in the emission wavelengths for ICLs grown on GaAs and Si (Fig. 4(c)). Our main hypothesis is related to a higher interface roughness for ICLs grown on mismatched substrates, which slightly changes the position of the quantum level in the W-QW and the emission. This interface roughness can be estimated from the RMS surface roughness measured on the AFM images (Fig. 2(b), 2(c) and 2(d)), which is eight times higher than on GaSb. However, this idea needs further investigation.

Finally, ageing measurements show that the ICLs do not degrade after 500 h of CW operation despite the high operating temperature (50°C) and injection current ($5xI_{th}$). These results demonstrate that dislocations do not significantly affect the device performance, and contrast with the outcomes observed for type-I QWs and QDs laser diodes (LDs). Indeed, in the case of QD lasers, such high TDDs reduce the reliability due to the dominance of carrier escape rates [28] which limit the measured lifetime to 800 h [29]. To improve the device performance, the TDD needs to be reduced to 10^6 - 10^7 cm^{-2} [28–30]. This is achieved through the use of annealing cycles and filter layers [22,29,31,32], which makes the buffer growth more complex.

Optics EXPRESS

When this strategy is applied to type-I QWs LDs, their performance remains limited [33] with a rapid degradation after 10 min of ageing at a defect density of $5 \times 10^7\,\mathrm{cm}^{-2}$ [34]. Thus, ICLs emerge as a promising design for interband lasers with high performance and long device lifetime on mismatched substrates.

7. Conclusion

In conclusion, we have successfully demonstrated high-performance ICLs grown simultaneously on GaSb, GaAs and Si substrates. Despite a TDD above $10^8\,\mathrm{cm}^{-2}$ in the mismatched structures, all the lasers exhibited comparable threshold currents around 40 mA with CW operation up to 65°C on all substrates. Furthermore, no degradation was observed after 500 h of ageing for ICLs on GaAs and Si at an injection current of 200 mA at 50°C. However, the high series resistance limits the maximum output power and will need to be improved in future work. These promising results pave the way for cost-effective integration of high-performance MIR lasers on large-sized mismatched substrates.

Funding. Agence Nationale de la Recherche (ANR-11-EQPX-0016, ANR-21-ESRE-0026); Région Occitanie Pyrénées-Méditerranée (LASIDO project); Agence de l'innovation de Défense; Bpifrance (Hyquality project DOS0188007/00).

Disclosures. The authors have no conflict to disclose.

Data availability. The data that support the findings of this study are available from the corresponding author upon reasonable request.

References

1. S.J. Sweeney, T.D. Eales, and I.P. Marko, eds. "The physics of mid-infrared semiconductor materials and heterostructures," in *Mid-Infrared Optoelectronics* E. Tournié and L. Cerutti, ed. (Elsevier, 2020).
2. H. Knötig, J. Nauschütz, N. Opačak, *et al.*, "Mitigating Valence Intersubband Absorption in Interband Cascade Lasers," Laser Photonics Rev. **16**(9), 2200156 (2022).
3. R. Q. Yang, L. Li, W. Huang, *et al.*, "InAs-Based Interband Cascade Lasers," IEEE J. Sel. Top. Quantum Electron. **25**(6), 1–8 (2019).
4. J. R. Meyer, W. W. Bewley, C. L. Canedy, *et al.*, "The Interband Cascade Laser," Photonics **7**(3), 75 (2020).
5. I. Vurgaftman, W. W. Bewley, C. L. Canedy, *et al.*, "Rebalancing of internally generated carriers for mid-infrared interband cascade lasers with very low power consumption," Nat. Commun. **2**(1), 585 (2011).
6. E. Tütüncü, M. Nägele, P. Fuchs, *et al.*, "iHWG-ICL: Methane Sensing with Substrate-Integrated Hollow Waveguides Directly Coupled to Interband Cascade Lasers," ACS Sens. **1**(7), 847–851 (2016).
7. C. Li, L. Dong, C. Zheng, *et al.*, "Compact TDLAS based optical sensor for ppb-level ethane detection by use of a 3.34μm room-temperature CW interband cascade laser," Sensors and Actuators B: Chemical **232**, 188–194 (2016).
8. P. Didier, H. Knötig, O. Spitz, *et al.*, "Interband cascade technology for energy-efficient mid-infrared free-space communication," Photonics Res. **11**(4), 582–590 (2023).
9. R. Ghorbani and F. M. Schmidt, "ICL-based TDLAS sensor for real-time breath gas analysis of carbon monoxide isotopes," Opt. Express **25**(11), 12743–12752 (2017).
10. E. Larson, M. Hines, M. Tanas, *et al.*, "Mid-infrared absorption by soft tissue sarcoma and cell ablation utilizing a mid-infrared interband cascade laser," J. Biomed. Opt. **26**(04), 043012 (2021).
11. Y. Shen, J. A. Massengale, R. Q. Yang, *et al.*, "Pushing the performance limits of long wavelength interband cascade lasers using innovative quantum well active regions," Appl. Phys. Lett. **123**(4), 041108 (2023).
12. Y. Han, H. Park, J. Bowers, *et al.*, "Recent advances in light sources on silicon," Adv. Opt. Photonics **14**(3), 404–454 (2022).
13. A. Spott, E. J. Stanton, A. Torres, *et al.*, "Interband cascade laser on silicon," Optica **5**(8), 996–1005 (2018).
14. L. Cerutti, D. A. Díaz Thomas, J.-B. Rodriguez, *et al.*, "Quantum well interband semiconductor lasers highly tolerant to dislocations," Optica **8**(11), 1397 (2021).
15. C. L. Canedy, W. W. Bewley, S. Tomasulo, *et al.*, "Mid-infrared interband cascade light emitting devices grown on off-axis silicon substrates," Opt. Express **29**(22), 35426–35441 (2021).
16. C. J. Hill and R. Q. Yang, "Interband cascade lasers grown on GaAs substrates lasing at 4 microns," Appl. Phys. Lett. **85**(15), 3014–3016 (2004).
17. J.-S. Park, M. Tang, S. Chen, *et al.*, "Heteroepitaxial Growth of III-V Semiconductors on Silicon," Crystals **10**(12), 1163 (2020).
18. R. Chandrasekar, Z. J. Lapin, A. Nichols, *et al.*, "Photonic integrated circuits for Department of Defense-relevant chemical and biological sensing applications: state-of-the-art and future outlooks," Opt. Eng. **58**(02), 1 (2019).
19. M. Rio Calvo, J.-B. Rodriguez, C. Cornet, *et al.*, "Crystal Phase Control during Epitaxial Hybridization of III-V Semiconductors with Silicon," Adv. Electron. Mater. **8**(1), 2100777 (2022).

Optics EXPRESS

20. A. Gilbert, M. Ramonda, L. Cerutti, *et al.*, "Epitaxial Growth of III-Vs on On-Axis Si: Breaking the Symmetry for Antiphase Domains Control and Burying," Adv. Opt. Mater. **11**(15), 2203050 (2023).
21. J. Selvidge, J. Norman, E. T. Hughes, *et al.*, "Defect filtering for thermal expansion induced dislocations in III–V lasers on silicon," Appl. Phys. Lett. **117**(12), 122101 (2020).
22. A. Y. Liu, R. W. Herrick, O. Ueda, *et al.*, "Reliability of InAs/GaAs Quantum Dot Lasers Epitaxially Grown on Silicon," IEEE J. Sel. Top. Quantum Electron. **21**(6), 690–697 (2015).
23. A. Remis, L. Monge-Bartolomé, G. Boissier, *et al.*, "Effect of dislocations on the performance of GaSb-based diode lasers grown on silicon," J. Appl. Phys. **133**(9), 093103 (2023).
24. J. Xia, F. Zhu, A. A. Kolomenskii, *et al.*, "Sensitive acetone detection with a mid-IR interband cascade laser and wavelength modulation spectroscopy," OSA Contin. **2**(3), 640–654 (2019).
25. D. A. Diaz-Thomas, O. Stepanenko, M. Bahriz, *et al.*, "Interband cascade Lasers with AlGaAsSb cladding layers emitting at 3.3 µm," Opt. Express **27**(22), 31425–31434 (2019).
26. B. Brar and D. Leonard, "Spiral growth of GaSb on (001) GaAs using molecular beam epitaxy," Appl. Phys. Lett. **66**(4), 463–465 (1995).
27. J.-S. Huang, "Reliability-extrapolation methodology of semiconductor laser diodes: is a quick life test feasible?" IEEE Trans. Device Mater. Relib. **6**(1), 46–51 (2006).
28. C. Shang, Y. Wan, J. Selvidge, *et al.*, "Perspectives on Advances in Quantum Dot Lasers and Integration with Si Photonic Integrated Circuits," ACS Photonics **8**(9), 2555–2566 (2021).
29. D. Jung, R. Herrick, J. Norman, *et al.*, "Impact of threading dislocation density on the lifetime of InAs quantum dot lasers on Si," Appl. Phys. Lett. **112**(15), 153507 (2018).
30. M. Buffolo, F. Samparisi, C. De Santi, *et al.*, "Physical Origin of the Optical Degradation of InAs Quantum Dot Lasers," IEEE J. Quantum Electron. **55**(3), 1–7 (2019).
31. D. Jung, Z. Zhang, J. Norman, *et al.*, "Highly Reliable Low-Threshold InAs Quantum Dot Lasers on On-Axis (001) Si with 87% Injection Efficiency," ACS Photonics **5**(3), 1094–1100 (2018).
32. E. Hughes, G. Kusch, J. Selvidge, *et al.*, "Dislocation-induced structural and luminescence degradation in InAs quantum dot emitters on silicon," Physica Status Solidi (a) **220**(14), 2300114 (2023).
33. M. Buffolo, C. De Santi, J. Norman, *et al.*, "A Review of the Reliability of Integrated IR Laser Diodes for Silicon Photonics," Electronics **10**(22), 2734 (2021).
34. C. Jiang, H. Liu, J. Wang, *et al.*, "Demonstration of room-temperature continuous-wave operation of InGaAs/AlGaAs quantum well lasers directly grown on on-axis silicon (001)," Appl. Phys. Lett. **121**(6), 061102 (2022).